NeuroImage: Clinical 30 (2021) 102619

Contents lists available at ScienceDirect

NeuroImage: Clinical

journal homepage: www.elsevier.com/locate/ynicl

Abnormal large-scale structural rich club organization in Leber's hereditary optic neuropathy

Jiahui Zhang (张佳慧)[a,1], Ling Wang (王玲)[b,1], Hao Ding (丁皓)[a,c], Ke Fan (范珂)[d], Qin Tian (田勤)[b], Meng Liang (梁猛)[a,c], Zhihua Sun (孙志华)[a,*], Dapeng Shi (史大鹏)[b,*], Wen Qin (秦文)[a,*]

[a] Department of Radiology & Tianjin Key Lab of Functional Imaging, Tianjin Medical University General Hospital, Tianjin 300052, China
[b] Department of Medical Imaging, Henan Provincial People's Hospital, Zhengzhou 450003, China
[c] School of Medical Imaging, Tianjin Medical University, Tianjin 300070, China
[d] Henan Eye Institute, Henan Eye Hospital, Zhengzhou University People's Hospital, Henan Provincial People's Hospital, Zhengzhou 450003, China

ARTICLE INFO

Keywords:
Leber's hereditary optic neuropathy
Structural network
Rich club
Diffusion tensor imaging
Duration
Retinal nerve fiber layer

ABSTRACT

Objective: The purpose of this study was to investigate whether the large-scale structural rich club organization was abnormal in patients with Leber's hereditary optic neuropathy (LHON) using diffusion tensor imaging (DTI), and the associations among disrupted brain structural connectivity, disease duration, and neuro-ophthalmological impairment.

Methods: Nineteen acute, 34 chronic LHON patients, and 36 healthy controls (HC) underwent DTI and neuro-ophthalmological measurements. The brain structural network and rich club organization were constructed based on deterministic fiber tracking at the individual level. Then intergroup differences among the acute, chronic LHON patients and healthy controls (HC) in three types of structural connections, including rich club, feeder, and local ones, were compared. Network-based Statistics (NBS) was also used to test the intergroup connectivity differences for each fiber. Several linear and nonlinear curve fit models were applied to explore the associations among large-scale brain structural connectivity, disease duration, and neuro-ophthalmological metrics.

Results: Compared to the HC, both the acute and chronic LHON patients had consistently significantly lower fractional anisotropy (FA) and higher radial diffusion (RD) for feeder connections ($p < 0.05$, FDR correction). Acute LHON patients had significantly lower FA and higher RD for local connections ($p < 0.05$, FDR correction). There was no significant difference in large-scale brain structural connectivity between acute and chronic LHON ($p > 0.05$, FDR correction). NBS also identified reduced FA of three feeder connections and five local ones linking visual, auditory, and basal ganglia areas in LHON patients ($p < 0.05$, FDR correction). No structural connections showed linear or nonlinear association with either disease duration or neuro-ophthalmological indicators ($p > 0.05$, FDR correction). A significant negative correlation was shown between the retinal nerve fiber layer (RNFL) thickness and disease duration ($p < 0.05$, FDR correction).

Conclusions: Abnormal rich club organization of the structural network was identified in both the acute and chronic LHON. Furthermore, our findings suggest the coexistence of both primary and secondary connectivity damage in the LHON.

Abbreviations: LHON, Leber's hereditary optic neuropathy; mtDNA, mitochondrial DNA; MD, mean defect; RNFL, retinal nerve fiber layer; MS, mean sensitivity; LV, loss of variance; NBS, network-based statistic; FA, fractional anisotropy; AD, axial diffusion; RD, radial diffusion.

* Corresponding authors at: Department of Radiology, Tianjin Medical University General Hospital, Anshan Road No. 154, Heping District, Tianjin 300052, China (Z. Sun and W. Qin). Department of Medical Imaging, Henan Provincial People's Hospital, Weiwu Road No. 7, Jinshui District, Zhengzhou, Henan Province, China (D. Shi).

E-mail addresses: dr_zhihuasun@sina.com (Z. Sun), cjr.shidapeng@vip.163.com (D. Shi), wayne.wenqin@gmail.com (W. Qin).

[1] These authors contributed equally to the manuscript.

https://doi.org/10.1016/j.nicl.2021.102619
Received 18 September 2020; Received in revised form 23 February 2021; Accepted 2 March 2021
Available online 8 March 2021

1. Introduction

Leber's hereditary optic neuropathy (LHON) is a mitochondrial genetic disease that is characterized by acute, painless, progressive loss of central vision with young male predominance (3 times than female) (Poincenot et al., 2020; Schaefer et al., 2008). Over 95% of LHON cases carry one of the three most common mitochondrial DNA (mtDNA) point mutations, including m.11778G > A, m.14484T > C, and m.3460G > A (Yu-Wai-Man et al., 2002). LHON patients usually suffer a quick loss of retinal ganglion cells (RGCs) and thinning of retinal nerve fiber layer (RNFL) thickness, as well as demyelination of optic nerve and loss of nerve fibers in the central part (Balducci et al., 2016; Carelli et al., 2002; Moster et al., 2016; Yu-Wai-Man et al., 2016). Besides the degeneration of the RGCs and optic nerves, previous studies had reported "visible" brain lesions in the LHON (Chang, 2018; Cui et al., 2020; Gropman et al., 2004; Mercuri et al., 2017; Nakaso et al., 2012). Advanced neuroimaging techniques such as high-resolution MRI, resting-state functional MRI (rs-fMRI), and diffusion tensor imaging (DTI) had also identified "invisible" abnormalities in brain gray and white matter (Barcella et al., 2010; Manners et al., 2015; Milesi et al., 2012; Rocca et al., 2011; Takemura et al., 2019). Finally, the functional reorganization of the associated visual areas (Vacchiano et al., 2019) was also reported.

It should be noted that these prior studies mainly focused on the local brain regions. The brain regions and their connectivity form a complex brain network (Bullmore and Sporns, 2009). Thus, functional and structural regional abnormalities in the LHON may also be accompanied by network abnormalities. One prior study based on 13 chronic LHON patients had reported functional reorganization in the visual and auditory networks (Rocca et al., 2011). However, the potential reorganization of the structural network in the LHON is still unknown. The rich club characterizes the network architecture that brain regions (hubs) with higher network degrees are very likely densely interconnected (Cai et al., 2019; van den Heuvel and Sporns, 2011). Three types of structural connections can be derived from the rich club organization, including rich club, feeder, and local connections (Collin et al., 2017). Based on early reports about the structural abnormalities in both the white matter and gray matter along the visual pathways (Barcella et al., 2010; Manners et al., 2015; Milesi et al., 2012; Rocca et al., 2011; Takemura et al., 2019), we hypothesized that the rich-club organization of the structural network in the LHON might also be involved.

It is also still unclear whether the network changes in LHON are secondary to visual impairment or may be caused by the primary effect of mitochondrial DNA (mtDNA) mutation itself. Brain structural and functional network reorganization secondary to visual impairment had been reported by many studies (Bola et al., 2014; Hasson et al., 2016; Li et al., 2013; Liu et al., 2007; Qin et al., 2015; Vacchiano et al., 2019; Wang et al., 2014). For the LHON, most reported brain abnormalities were related to the visual pathways (Barcella et al., 2010; Manners et al., 2015; Milesi et al., 2012; Rocca et al., 2011; Takemura et al., 2019). Thus, the secondary involvement of the brain network hypothesis can be made from the above findings. However, there were also some pieces of evidence supporting the primary involvement in the LHON. Such as neurological symptoms and lesions that cannot be explained by visual impairment (Cui et al., 2020; Rance et al., 2012; Saracchi et al., 2013), as well as white matter (Long et al., 2019) and metabolism (Ostojic et al., 2009) abnormalities in asymptotic LHON carriers. To elucidate the issue, we investigate the effect of disease duration on rich-club structural network changes in LHON patients.

In the present study, we recruited a relatively large cohort of acute and chronic LHON patients with normal-appearing brain tissue without other clinical symptoms except for vision loss. The DTI images were used to construct the rich-club organization of the large-scale structural network (Jeurissen et al., 2019). To figure out whether LHON disrupted the rich club organization of the structural network, we compared intergroup differences in rich-club connectivity between LHON patients and healthy controls (HC). Network-based Statistics (NBS) were also used to identify which fiber branches were involved (Zalesky et al., 2010). Finally, several linear and nonlinear curve fit models were applied to explore the potential associations among rich club connectivity, disease duration, and neuro-ophthalmological metrics.

2. Materials and methods

2.1. Participants

We prospectively recruited 55 LHON patients diagnosed in Zhengzhou University People's Hospital from May 2012 to December 2016. Inclusion criteria were: (1) carried one of the three main mtDNA point mutations associated with LHON (m.11778G > A, m.14484T > C, m.3460G > A); (2) characterized by acute or subacute, painless loss of central vision and excluded other optic neuropathies such as glaucoma and cataract, and so on; (3) without a history of neurological, psychiatric, major medical conditions or substance abuse; (4) without intracranial or intra-orbital lesions on T2-weighted images. An acute LHON patient was excluded due to the inability to cooperate with the neuro-ophthalmological examination. A chronic LHON patient was excluded on account of the absence of T1 weighted images. Therefore, this study finally enrolled 19 acute LHON patients (duration <12 months, ages ranging from 10 years to 57 years old, 17 males, 14 cases of m.11778G > A, and 5 cases of m.14484T > C), and 34 chronic LHON patients (duration ≥12 months, ages ranging from 13 years to 53 years old, 23 males, 27 cases of m.11778G > A, 4 cases of m.14484T > C and 3 cases of m.3460G > A). The 53 LHON covered a wide range of disease duration spanning the acute and chronic phases (from 3 weeks to 422 months). All patients had normal-appearing brain tissue without other clinical symptoms except for vision loss. All patients had been treated with idebenone during the acute phase for 1 week to 3 months before the MRI examination. We also initially recruited 38 healthy controls (HC) with the same inclusion criteria as LHON except for the absence of visual abnormality and no evidence of mtDNA mutations. The MRI data of the HC were scanned within a similar time range as the LHON patients. Two of them were excluded due to severe head motion artifacts. Therefore, 36 healthy controls were finally enrolled in the present study (ages ranging from 9 years to 44 years old, 26 males). Ten acute LHON patients, 6 chronic LHON patients, and 7 healthy controls were below 18 years old. The detailed demographic information was provided in Table 1. It should be commented that the diffusion tensor images (DTI) of 15 healthy control (HC) in the present study overlapped with an earlier study that aimed to detect the abnormality in white matter integrity in non-symptomatic LHON carriers (Long et al., 2019). There were also 25 chronic LHON patients and 28 HC that overlapped with another study that focuses on the optic nerve alterations (Wang et al., 2017). However, the work by Wang et al. used different DTI scans (imaging the optic nerves); thus, there was no overlapped data between the present study and that by Wang et al. Finally, the contents in the present study had no overlap with the early two studies.

This study was approved by the Ethics Committees of Henan Provincial People's Hospital. The experimental procedure followed the Code of Ethics of the World Medical Association (Declaration of Helsinki). Written informed consent was obtained from each subject or his/her parents (if age <18 years old) before the study.

2.2. Neuro-ophthalmological examination

The corrected visual acuity was evaluated by the logarithm of the minimum angle of resolution (logMAR). We obtained the visual field by using Octopus perimeter 101G2 program TOP Strategy (Interzeag AG, Haig-Streit Schlieren, Switzerland) and mean defect (MD), mean sensitivity (MS), and loss of variance (LV) of the visual field. The average thickness of the peripapillary RNFL thickness was measured by a high-resolution spectral-domain optical coherence tomography (Carl Zeiss Meditec, Dublin, CA, USA) with a diameter of 3.45 mm.

Table 1
Demographic and clinical characteristics of this study.

	Acute LHON	Chronic LHON	HC	Total effects		Acute vs chronic	Acute vs HC	chronic vs HC
				$F/T/\chi^2$	p	p	p	p
Age (years)	21.37 ± 11.62	26.85 ± 11.69	24.31 ± 9.63	$F = 1.563$	$p = 0.215$	–	–	–
Gender (Male/Female)	17/2	23/11	26/10	$\chi^2 = 3.148$	$p = 0.207$	–	–	–
Duration (months)	3.25 ± 2.62	113.65 ± 127.00	–	***T = -3.772***	***p = 4.220e^{-4}***	–	–	–
MD (dB)	12.87 ± 9.26	17.84 ± 8.05	1.56 ± 1.04	***F = 46.989***	***p = 5.904e^{-14}***	***p = 0.019***	***p = 1.000e^{-6}***	***p = 1.058e^{-14}***
MS (dB)	16.35 ± 7.77	11.22 ± 8.18	27.56 ± 1.17	***F = 52.419***	***p = 8.940e^{-15}***	***p = 0.019***	***p = 2.000e^{-6}***	***p = 1.447e^{-15}***
LV (dB^2)	23.22 ± 26.83	36.80 ± 24.64	4.05 ± 1.97	***F = 21.325***	***p = 5.086e^{-8}***	***p = 0.039***	***p = 0.005***	***p = 7.780e^{-9}***
RNFL thickness(μm)	108.50 ± 24.28	63.48 ± 18.61	100.62 ± 6.66	***F = 54.082***	***p = 2.872e^{-15}***	***p = 2.637e^{-13}***	$p = 0.131$	***p = 1.001e^{-12}***
mtDNA.11778G > A	14	27	–	$p = 0.230$*		–	–	–
mtDNA.14484T > C	5	4	–			–	–	–
mtDNA.3460G > A	0	3	–			–	–	–

Note: p values highlighted in bold plus italics indicate statistical significance ($p < 0.05$, FDR correction). *Fisher's exact test.
Abbreviations: LHON = Leber's hereditary optic neuropathy; HC = Healthy controls; MD = Mean defect; MS = Mean sensitivity; LV = Loss of variance; RNFL = Retinal nerve fiber layer; mtDNA = Mitochondrial DNA.

2.3. MRI data acquisitions

Brain MRI data were obtained by a 3.0 T MR scanner (Discovery MR750, GE Healthcare, Waukesha, WI, USA). Participants with intracranial or intra-orbital lesions were excluded via a T2-weighted fast spin-echo (FSE) sequence with the following imaging parameters: repetition time (TR) = 8674 ms, echo time (TE) = 93 ms, thickness = 6 mm, field of view (FOV) = 240 × 240 mm, gap = 1.5 mm, and slices = 18. High-resolution three-dimensional T1-weighted (T1W) images were obtained using a fast-spoiled gradient echo sequence. The scan parameters were: TE = 3.2 ms, TR = 8.2 ms, inversion time (TI) = 450 ms, FOV = 256 mm × 256 mm; matrix = 256 × 256, slice thickness = 1 mm without gap, and 176 slices. DTI data were acquired using a diffusion-weighted spin-echo single-shot echo-planar imaging (EPI) sequence with one baseline volume without diffusion gradient and 30 diffusion encoding directions (b = 1000 s/mm^2). Other scan parameters included: TE = 90 ms, TR = 8000 ms, FOV = 256 mm × 256 mm, matrix = 128 × 128, slice thickness = 3 mm without gap, and 48 slices.

2.4. Data analysis

2.4.1. Data preprocessing for DTI and deterministic fiber tracking

We processed DTI data by utilizing the PANDA toolbox (Version 1.3.1, http://www.nitrc.org/projects/panda), which was a combination of the FMRIB Software Library (FSL version 5.0.10, http://fsl.fmrib.ox.ac.uk/fsl/fslwiki) and the Diffusion Toolkit (DTK version 0.6.4.1, http://www.trackvis.org/dtk). As for data preprocessing, we followed up with the steps: converting DICOM images into NIFTI format, extracting brain, correcting eddy current, eliminating head motion artifacts, estimating tensor using a linear least-squares fitting method, calculating DTI metrics including fractional anisotropy (FA), axial diffusivity (AD) and radial diffusivity (RD). Then we carried out whole brain deterministic fiber tracking using fiber assignment by continuous tracking algorithm (FACT) with a turned angle >80° and FA <0.15 within a predefined brain mask. We estimated the deformation from individual diffusion space to Montreal Neurological Institute (MNI) space by the following steps: First, each subject's b0 map was linearly coregistered into his/her T1W image. Then the individual T1W images were nonlinearly normalized into MNI space by FNIRT (FMRIB's nonlinear registration Tool). Finally, the deformation parameters for these two steps were concatenated to inversely warp the atlas from MNI to individual space to extract the fibers between each pair of brain regions.

2.4.2. Brain structural network construction

The brain structural network was constructed using the PANDA (Version 1.3.1, http://www.nitrc.org/projects/panda) and the GRETNA toolbox (Version 2.0, http://www.nitrc.org/projects/gretna/). The Human Brainnetome Atlas (Fan et al., 2016) was used to define the network nodes. This atlas was first warped into individual diffusion space using the deformation parameters generated at the preprocessing steps. Then fibers between each pair of seeds were extracted. If there were at least 3 fibers between the two nodes, their connectivity (network edge) was considered to exist. It had been reported that the rich club nodes are characterized by a high degree, low clustering, short path length, high centrality, and high participation in multiple communities across the whole brain network (Cai et al., 2019; van den Heuvel and Sporns, 2011). To identify the rich club hubs, all network nodes were ranked according to the degree (K) at the individual level. We selected the top 12% (30 nodes out of the whole 246 brain regions) of most consistently ranked nodes as rich club hubs across all 36 HC (van den Heuvel et al., 2013), which corresponding to median K = 15 (interquartile ranges from 14 to 16) at the individual level (Supplementary Table 1). We calculated the normalized rich club coefficient (φ^{W}_{Norm}) using the FA at the individual level with 1000 random network permutations. In GRETNA, the random networks are generated by a Markov wiring algorithm (Maslov and Sneppen, 2002), which preserves the same number of nodes and edges and the same degree distribution as real brain networks. Finally, three types of connections were calculated based on the categorization of the network nodes (rich club or non-rich club nodes): rich club, feeder, and local connections. Rich club connections connect rich club nodes. They play a pivotal role in global communication. Damage to these links would cause a significant decrease in global network efficiency. Local connections link non-rich club nodes. They are closely associated with local communication. Damage to them would cause a reduction in local network efficiency rather than the global one. Feeder connections bridge the rich and non-rich club nodes. They play important roles in communicating between the rich and non-rich club sub-networks (van den Heuvel and Sporns, 2011).

2.4.3. Statistical analyses

We first compared intergroup differences among acute, chronic LHON patients and HC in φ^{W}_{Norm} using a fixed-effect general linear model (GLM) after regressing out the effects of gender and age ($p < 0.05$, false discovery rate [FDR] correction). Intergroup differences in diffusion metrics (including the FA, AD, and RD) of the rich club, feeder, and local connections were also compared using the GLM model after regressing out covariates of gender and age ($p < 0.05$, FDR correction) by SPSS 24.0 (https://www.ibm.com/analytics/spss-statistics-software). We additionally compared the diffusion metrics among different subtypes of LHON mutations using a fixed-effect general linear model (GLM) after regressing out the effects of age and gender ($p < 0.05$, FDR correction). Furthermore, in order to identify significantly abnormal connections in each pair of brain regions, a network-based statistic (NBS) analysis was carried out between the LHON patients

and healthy controls (10,000 non-parametric permutations, edge-level $p < 0.001$, corrected $p < 0.05$) after regressing out covariates of gender and age (Zalesky et al., 2010) by GRETNA toolbox V2.0.0 (http://www.nitrc.org/projects/gretna/). Curve fits including linear, logarithmic, power, and exponential models were performed among the disrupted brain structural connectome, disease duration, and neuro-ophthalmological metrics, respectively, after regressing covariates gender and age ($p < 0.05$, FDR correction).

2.5. Sensitivity analysis

To test the result's reliability, we also define the network nodes using the Anatomical Automatic Labeling (AAL) atlas. The connectivity and rich club architecture were defined using the same way mentioned in the "*Brain structural network construction*" section. Finally, 11 nodes (12%) out of the whole 90 cerebral brain regions were defined as the rich club nodes. We then calculated the three types of structural connections and carried out the statistical analysis as mentioned above ($p < 0.05$, FDR correction).

3. Results

3.1. Demographic and clinical characteristics

The demographic and clinical characteristics of our study were summarized in Table 1. No statistical differences were found in age (analysis of variance [ANOVA], $F = 1.563$, $p = 0.215$) and gender (Chi-square test, $\chi^2 = 3.148$, $p = 0.207$) among the acute LHON, chronic LHON patients and the HC. ANOVA revealed significant differences in MD ($F = 46.989$, $p = 5.904e^{-14}$), MS ($F = 52.419$, $p = 8.940e^{-15}$), LV ($F = 21.325$, $p = 5.086e^{-8}$), and RNFL thickness ($F = 54.082$, $p = 2.872e^{-15}$) among the acute LHON, chronic LHON, and the HC. Post hoc analysis demonstrated acute LHON patients had higher MD ($p = 1.000e^{-6}$), higher LV ($p = 0.005$) and lower MS ($p = 2.000e^{-6}$) than the HC. Chronic LHON patients had higher MD ($p = 1.058e^{-14}$), higher LV ($p = 7.780e^{-9}$), lower MS ($p = 1.447e^{-15}$) and thinner RNFL thickness ($p = 1.001e^{-12}$) than the HC. Besides, chronic LHON patients had higher MD ($p = 0.019$), higher LV ($p = 0.039$), lower MS ($p = 0.019$) and thinner RNFL thickness ($p = 2.637e^{-13}$) than the acute LHON. No RNFL

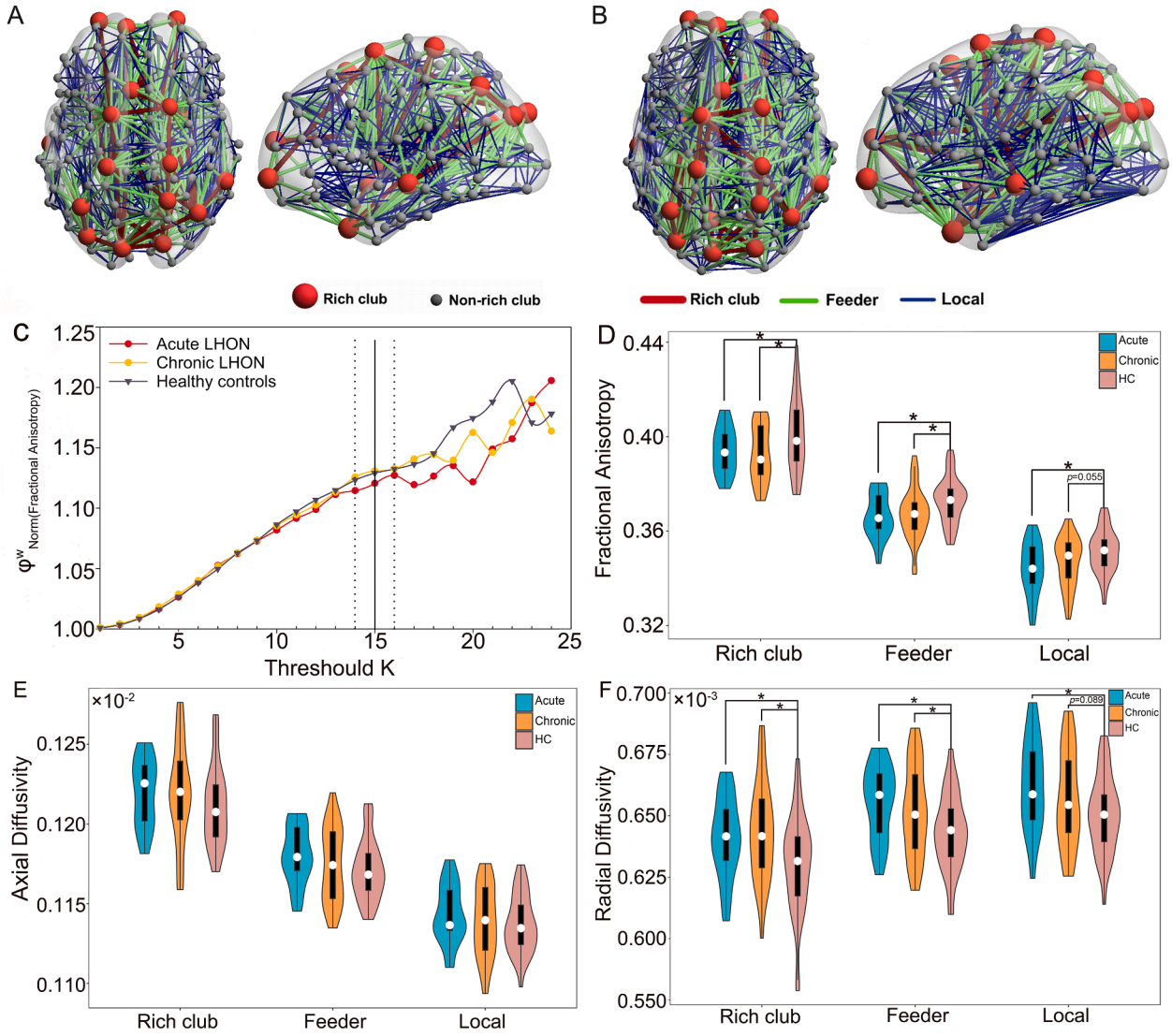

Fig. 1. Rich club organization and intergroup comparison in brain structural connectome. Rich club organization of structural network in (A) one Leber's hereditary optic neuropathy (LHON) patient and (B) one healthy control (HC) visualized using Brainnet Viewer version 1.7 (https://www.nitrc.org/projects/bnv/). (C) The mean normalized rich club coefficients based fractional anisotropy values were calculated at the individual level for acute, chronic LHON, and HC groups. Solid and dash line represents the median and interquartile range, respectively. Intergroup differences among acute LHON, chronic LHON, and HC in (D) fractional anisotropy, (E) axial diffusivity, and (F) radial diffusivity (RD) of rich club, feeder, and local connections were shown through the violin diagrams. Asterisk (*) represents statistical significance corrected using false discovery rate (FDR) correction ($p < 0.05$).

thickness difference was found between acute LHON patients and the HC ($p = 0.131$). No significant difference was found in the number of patients of three types of mtDNA mutation patients between acute and chronic LHON (Fisher's exact test, $p = 0.230$).

3.2. Changes in rich club organization of structural network

The example of rich club organization in one LHON and one HC individual based on Brainnetome Atlas can be seen in Fig. 1A and B. The detailed information of the 30 rich club nodes was listed in Supplementary Table 1. The intergroup differences in normalized rich club coefficients were not significant among the acute, chronic LHON, and HC ($p > 0.05$, FDR correction) (Fig. 1C). Regarding the three types of structural connections, there were significant differences in FA (Fig. 1D) and RD (Fig. 1F) among the three groups ($p < 0.05$, FDR correction), but missing differences in AD (Fig. 1E) ($p > 0.05$, FDR correction) (Table 2). Post hoc analysis showed that acute LHON had lower FA for the rich club, feeder, and local connections (Fig. 1D, Table 2), and higher RD for the rich club, feeder, and local connections than the HC ($p < 0.05$, FDR correction) (Fig. 1F, Table 2). Similarly, chronic LHON had significantly lower FA for the rich club and feeder connections (Fig. 1D, Table 2) and higher RD for the rich club and feeder ($p < 0.05$, FDR correction) (Fig. 1F, Table 2). Chronic LHON also showed marginal lower FA for local connections ($p = 0.055$, uncorrected) and higher RD for local connections ($p = 0.089$) than the HC (Fig. 1D, F, Table 2). There was no intergroup difference in diffusion metrics of each connection type between acute and chronic LHON ($p > 0.05$, FDR correction, Table 2, Fig. 1D–F). We did not find significant differences in diffusion metrics of either connectivity type among the three types of mtDNA mutations (Supplementary Table 2).

During the NBS analysis, because no statistical difference in diffusion metrics was found between the acute and chronic LHON, we merged the two LHON subgroups and tested which fibers were disrupted in the LHON. NBS analysis identified an abnormal connectivity cluster with decreased FA (edge-level $p < 0.001$, corrected $p < 0.05$), which included 3 feeder and 5 local connections that connected the dorsal and ventral visual, auditory, and basal ganglia areas (Fig. 2 and Supplementary Table 3).

3.3. Correlations among disrupted large-scale structural connectivity, disease duration, and neuro-ophthalmological measures

There were no statistically linear or nonlinear correlations between the diffusion metrics of disrupted large-scale brain structural connectivity and neuro-ophthalmological measures (including the MD, LV, RNFL thickness, and MS) in either acute or chronic LHON patients using any of linear, logarithmic, power, and exponential curve fitting models ($p > 0.05$, FDR correction) (Supplementary Tables 4–11). There were also no significant correlations between disrupted large-scale brain structural connectivity and disease duration of all LHON patients in either model ($p > 0.05$, FDR correction, Supplementary Table 12). It showed significant negative correlation between the disease duration and RNFL thickness with most significance using exponential nonlinear fit model ($R^2_{adj} = 0.503$, β = -0.117, $p = 3.900e^{-8}$, FDR correction, Fig. 3, Supplementary Table 13).

Table 2
Intergroup differences in diffusion metrics of structural network among acute, chronic LHON, and HC.

Connectivity	Total Effects		Pairwise comparisons (p values)		
	F	p	Acute vs. HC	Chronic vs. HC	Acute vs. Chronic
Rich club FA	3.824	***0.026***	***0.041***	***0.015***	0.987
Feeder FA	5.006	***0.009***	***0.008***	***0.013***	0.547
Local FA	4.334	***0.016***	***0.006***	0.055*	0.257
Rich club AD	0.866	0.425	0.382	0.217	0.875
Feeder AD	0.938	0.395	0.193	0.384	0.574
Local AD	0.342	0.712	0.490	0.496	0.905
Rich club RD	4.702	***0.012***	***0.036***	***0.005***	0.800
Feeder RD	4.980	***0.009***	***0.007***	***0.017***	0.470
Local RD	3.142	***0.048***	***0.021***	0.089*	0.380

Note: p values highlighted in bold plus italics indicate statistical significance ($p < 0.05$, FDR correction). * represented marginal significance. Abbreviations: LHON = Leber's hereditary optic neuropathy, HC = healthy control, FA = fractional anisotropy, AD = axial diffusivity, RD = radial diffusivity.

3.4. Sensitivity results based on AAL atlas

We reconstruct the rich club network architecture using the AAL atlas. We also found significant differences in FA of the feeder and local connections (Supplementary Fig. 1A), and significant differences in RD of the feeder and local connections (Supplementary Fig. 1C) among the acute, chronic LHON, and HC ($p < 0.05$, FDR correction), but missing differences in FA and RD of the rich club connections, and in AD of all types of connections among the groups ($p > 0.05$, FDR correction) (Supplementary Fig. 1, Supplementary Table 14). Post hoc analysis showed that the acute LHON had significantly lower FA for feeder and local connections ($p < 0.05$, FDR correction), (Supplementary Fig. 1A, Supplementary Table 14), higher RD for feeder and local connections than the HC ($p < 0.05$, FDR correction) (Supplementary Fig. 1C, Supplementary Table 14). Similarly, chronic LHON had marginal lower FA for feeder and local connections ($p < 0.05$, uncorrected) (Supplementary Fig. 1A, Supplementary Table 14), higher RD for feeder ($p = 0.051$, marginal significance) and local connections ($p = 0.022$, FDR correction), (Supplementary Fig. 1C, Supplementary Table 14) compared to the HC. Furthermore, there was no intergroup difference in diffusion metrics between acute and chronic LHON in each type of structural connections ($p > 0.05$, FDR correction), Supplementary Table 14).

Curve fitting analysis demonstrated that the structural connectivity showed no linear or nonlinear association with either disease duration or neuro-ophthalmological indicators in acute or chronic LHON ($p > 0.05$, FDR correction, Supplementary Tables 15–23).

4. Discussion

In this study, we recruited a relatively large cohort of LHON patients to elucidate the potential changes in the structural network's rich club organization. We found no differences in rich club coefficients among the acute, chronic LHON, and HC. Using different atlases, we identified that the disrupted large-scale brain structural connections in acute and chronic LHON were consistently ascribed to the feeder and local connections. No intergroup difference in connectivity disruption was found between acute and chronic LHON. The involved structural connectivity showed no linear or nonlinear association with the disease duration and ophthalmological impairment. These findings suggested a disrupted rich club organization of the structural network in the LHON.

The present study's main finding was that the non-rich club organization of structural network was involved in LHON patients. No intergroup differences in normalized rich club coefficients were found among the acute, chronic LHON patients and HC, indicating relative preservation of the rich club organization in the LHON. Although the acute and chronic LHON patients showed changed rich club connectivity when the network was constructed using the Brainnnetome Atlas, this result failed validation when using an AAL Atlas. In contrast, both Atlases consistently identified reduced FA and increased RD of the feed and local connections in the two subgroups of LHON patients. Coupled with the result of NBS analysis that identified reduced FA in 3 feeder and 5 local connections in LHON patients, these findings suggest that abnormal large-scale structural connectivity in LHON mainly involved peripheral non-rich club components. Reduced FA and increased RD might indicate demyelination or loss of axonal density in these tracts (Qin et al., 2012). It should be noted that a higher RD trend was

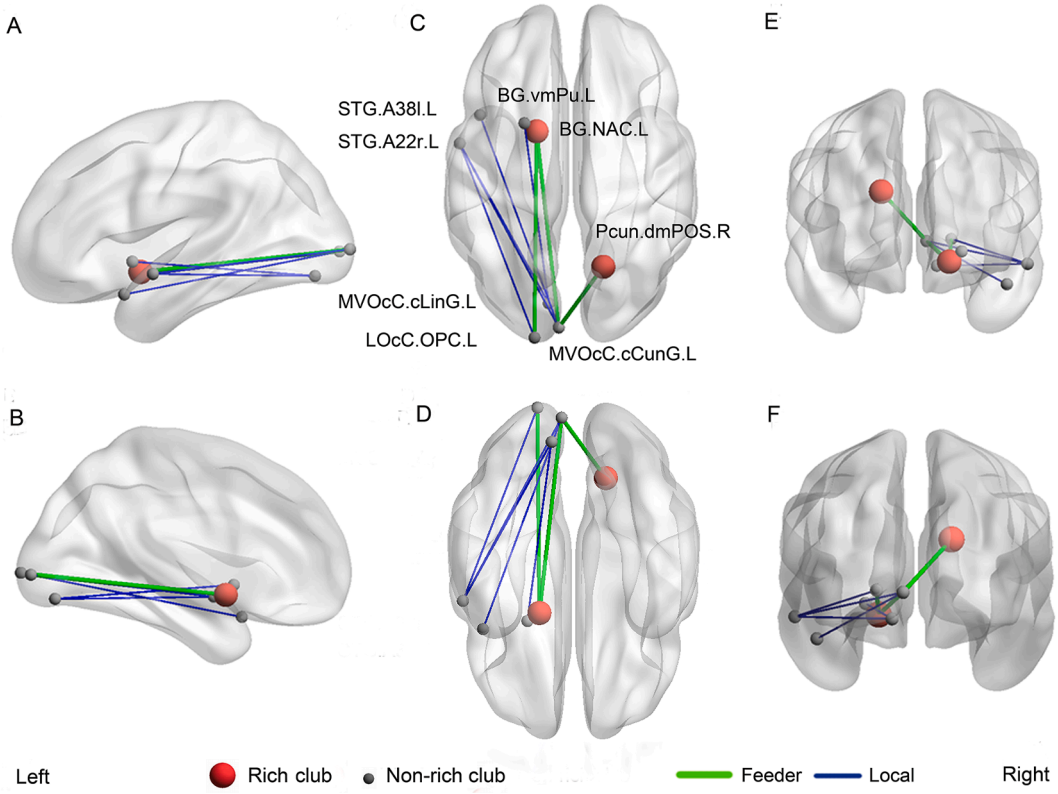

Fig. 2. Intergroup differences in fractional anisotropy (FA) for each connection using network-based statistics (NBS). NBS identified a connectivity cluster with significantly decreased FA for LHON patients (10000 non-parametric permutation, edge $p < 0.001$, corrected $p < 0.05$). (A) Left hemisphere sagittal outside view. (B) Left hemisphere sagittal inside view. (C) Cerebrum axial superior view. (D) Cerebrum axial inferior view. (E) Cerebrum coronal anterior view. (F) Cerebrum coronal posterior view. Abbreviations: STG.A38l.L = lateral area 38 of left superior temporal gyrus; STG.A22r.L = rostral area 22 of left superior temporal gyrus; Pcun.dmPOS.R = dorsomedial parietooccipital sulcus of right precuneus; MVOcC.cLinG.L = caudal lingual gyrus left medioventral occipital cortex; MVOcC.cCunG.L = caudal cuneus gyrus of left medioventral occipital cortex; LOcC.OPC.L = occipital polar cortex of left lateral occipital cortex; BG.NAC.L = nucleus accumbens of left basal ganglia; BG.vmPu.L = ventromedial putamen of left basal ganglia.

observed in the acute LHON than the chronic LHON and HC (Fig. 1F), which might be implausible to suggest axonal "demyelination" in the acute LHON. Peripapillary RNFL and optic disc edema, and radial peripapillary capillaries hyperemia were evident in the acute LHON (Gaier et al., 2016; Mejia-Vergara et al., 2020). Thus, the trend of increased RD and AD (see Fig. 1E and F) in the acute LHON may be explained by increased extracellular space caused by edema at the early stage. Because there was no statistical significance for these tests, this explanation should be validated with a larger sample size in the future.

These non-rich club structural dysconnectivity mainly link the dorsal visual, ventral visual, auditory, and basal ganglia regions. Our findings were consistent with previous reports regarding impairments inside and outside the visual pathways of LHON (Barcella et al., 2010; Ceranic and Luxon, 2004; Cui et al., 2020; Gropman et al., 2004; Leng et al., 2015; Manners et al., 2015; Mercuri et al., 2017; Milesi et al., 2012; Ogawa et al., 2014; Rance et al., 2012; Rizzo et al., 2012; Takemura et al., 2019; Yu-Wai-Man et al., 2008). Interestingly, most involved brain nodes are ascribed to peripheral "processing" systems that undertake visual/auditory sensation and motor controlling (Swenson, 2006). These findings can explain the sensorimotor symptoms found in few LHON patients. A meta-analysis with 26 kinds of neurological or psychiatric diseases had revealed that diseases that involved high-cognitive "control system" would more likely damage rich club hubs (such as frontotemporal dementia, schizophrenia, epilepsy, post-traumatic stress disorder, and Alzheimer's disease). In contrast, diseases that mainly involved the sensorimotor "process system" would more likely have intact non-rich club hubs (such as multiple sclerosis, Parkinson's disease, dystonia, ataxia, and pain) (Crossley et al., 2014). Thus, our findings suggested that the peripheral "process system" might be more vulnerably affected by LHON disease.

In the present study, the involved LHON patients covered a wide range of disease duration spanning the acute and chronic phases (from 3 weeks to 422 months). We observed a significantly negatively nonlinear association between the disease duration and RNFL thickness, indicating that the degeneration of RGCs and their axons were fast at the early symptomatic stage while kept relatively stable later, as shown in early longitudinal observations (Balducci et al., 2016). However, we did not find any association between the disrupted brain structural connectivity and disease duration, or missing association between the structural connectivity and ophthalmological metrics (including the RNFL thickness) no matter using linear, logarithmic, power, and exponential fit models. Furthermore, there was no intergroup difference in structural connectivity integrity between acute and chronic LHON patients. These findings may be explained by the primary involvement of structural connections in LHON. Similarly, some previous studies had illustrated that the microstructure and metabolism of brain white matter were changed in asymptomatic LHON carriers (Long et al., 2019; Ostojic et al., 2009). Neurological symptoms and lesions unrelated to the visual system were also reported (Cui et al., 2020; Rance et al., 2012; Saracchi et al., 2013). However, in the present study, NBS analysis demonstrated that most disrupted connections involved the visual areas. Early studies have also reported that the post-geniculate visual pathway has degenerated in the chronic LHON (Barcella et al., 2010; Manners et al., 2015; Milesi et al., 2012; Rocca et al., 2011; Takemura et al., 2019). Thus, secondary degeneration may also partly explain the damaged peripheral connections after LHON, especially for chronic patients. It should be noted that we defined the structural network using DTI. Because there are big gaps between the DTI-derived network topology and the

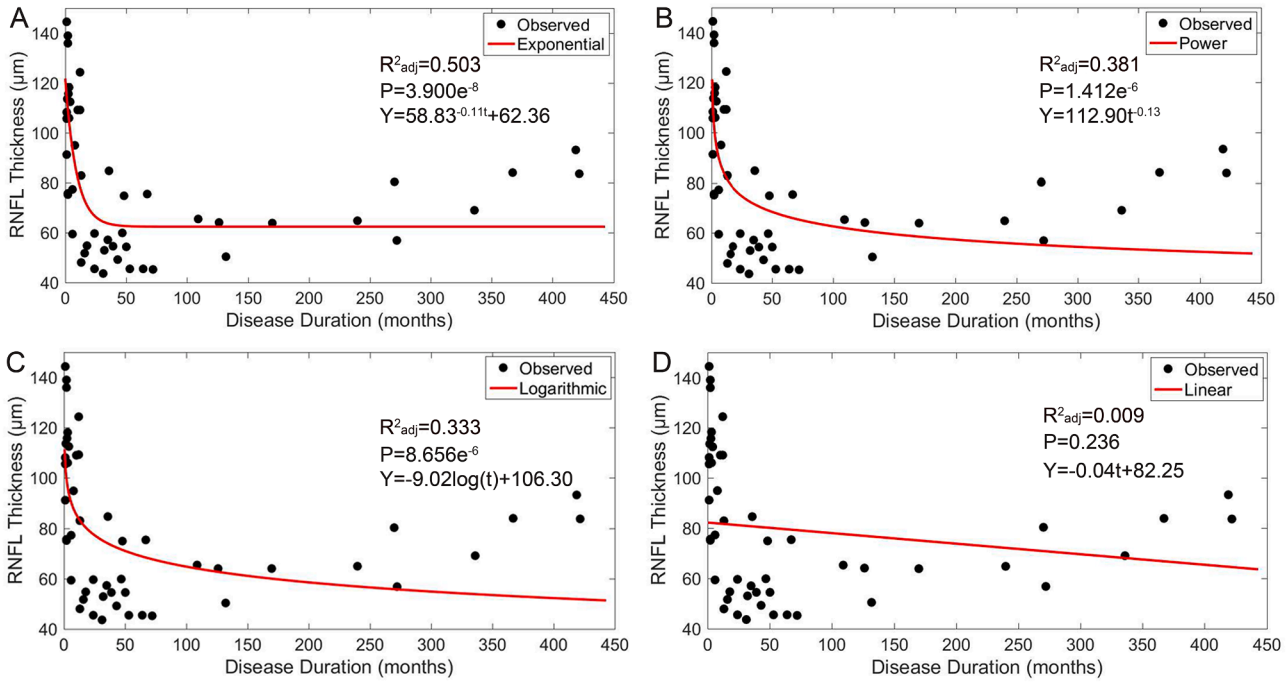

Fig. 3. Correlation between the disease duration and RNFL thickness in the LHON. There showed a significantly negative correlation between the disease duration and RNFL thickness in the LHON no matter using (A) exponential, (B) power, and (C) logarithmic fit models, with the highest adjusted R-square (R^2_{adj}) for the exponential model. No correlation was found by using (D) linear fit model. The effects of age and gender had been regressed out from the RNFL thickness before correlation. Abbreviation: RNFL = retinal nerve fiber layer, LHON = Leber's hereditary optic neuropathy.

biological structural network composed of neurons and their axons, it is sensitive to many of the methodological choices and assumptions (Buchanan et al., 2020; Schiavi et al., 2020). Thus, the DTI-derived network may reflect only a part of the properties of the large-scale brain network (Kim and Min, 2020). We also found that there was a significant nonlinear association between the RNFL thickness and disease duration; however, DTI-derived feeder and local connectivity measures failed to identify similar mode, which may be ascribed by the following factors: DTI-derived connectivity measures are not sensitive enough to detect the degeneration of occipital connectivity, or secondary axonal degeneration of the visual cortex is weaker than the RNFL.

There were several limitations to the present study. First, the DTI data were acquired using only one b0 (baseline) and 30 diffusion encoding directions, which were not sufficient to precisely assess the diffusion metrics (Farrell et al., 2007; Zhan et al., 2010) and resolve crossing fibers (Maier-Hein et al., 2017; Yeh et al., 2020). Second, the field mapping or phase-flipped images were not acquired to correct susceptibility-induced artifacts, influencing the connectivity findings near the temporal pole and orbitofrontal cortex. Third, previous studies had reported sex differences in rich-club metrics (Wang et al., 2019). LHON belongs to a kind of rare disease with a 3:1 male: female ratio, meaning that female LHON patients are rarer than male ones (Lissa Poincenot, 2019). It is difficult to keep a balance between the number of male and female LHON patients. In the present study, only 2 females were enrolled in acute LHON, and it is unreliable to elucidate the effect of gender on rich-club metrics changes. A larger sample size is needed to clarify this issue in the future. Fourth, we only focused on measuring the function of the vision system. It was a pity that we did not design elaborate cognition, sensory, and motor tasks to associate brain network disruption with these functions.

In summary, we found that the large-scale structural network of LHON patients was impaired, which mainly involved the non-rich club process system. Furthermore, our findings suggest the coexistence of both primary and secondary connectivity damage in the LHON.

Funding

This work was supported by the Natural Science Foundation of China (81771818, 81971599, 81971694, 81601473), Natural Science Foundation of Tianjin City (19JCYBJC25100, 17JCYBJC29200), Postdoctoral Science Foundation of China (2017M611175).

CRediT authorship contribution statement

Jiahui Zhang: Formal analysis. **Ling Wang:** Conceptualization, Investigation, Project administration. **Hao Ding:** Formal analysis. **Ke Fan:** Investigation. **Qin Tian:** Investigation. **Meng Liang:** Formal analysis. **Zhihua Sun:** Conceptualization. **Dapeng Shi:** Conceptualization, Investigation, Resources. **Wen Qin:** Conceptualization, Formal analysis.

Declaration of Competing Interest

The authors declare that they have no known competing financial interests or personal relationships that could have appeared to influence the work reported in this paper.

Acknowledgements

We appreciated members of the Department of Radiology & Tianjin Key Lab of Functional Imaging of Tianjin Medical University General Hospital for their technical support. We also appreciated members of the Department of Radiology of Henan Provincial People's Hospital for data collection.

Appendix A. Supplementary data

Supplementary data to this article can be found online at https://doi.org/10.1016/j.nicl.2021.102619.

References

Balducci, N., Savini, G., Cascavilla, M.L., La Morgia, C., Triolo, G., Giglio, R., Carbonelli, M., Parisi, V., Sadun, A.A., Bandello, F., Carelli, V., Barboni, P., 2016. Macular nerve fibre and ganglion cell layer changes in acute Leber's hereditary optic neuropathy. Br. J. Ophthalmol. 100 (9), 1232–1237. https://doi.org/10.1136/bjophthalmol-2015-307326.

Barcella, V., Rocca, M.A., Bianchi-Marzoli, S., Milesi, J., Melzi, L., Falini, A., Pierro, L., Filippi, M., 2010. Evidence for retrochiasmatic tissue loss in Leber's hereditary optic neuropathy. Hum. Brain Mapp. 31, 1900–1906. https://doi.org/10.1002/hbm.20985.

Bola, M., Gall, C., Moewes, C., Fedorov, A., Hinrichs, H., Sabel, B.A., 2014. Brain functional connectivity network breakdown and restoration in blindness. Neurology 83, 542–551. https://doi.org/10.1212/WNL.0000000000000672.

Buchanan, C.R., Bastin, M.E., Ritchie, S.J., Liewald, D.C., Madole, J.W., Tucker-Drob, E. M., Deary, I.J., Cox, S.R., 2020. The effect of network thresholding and weighting on structural brain networks in the UK Biobank. Neuroimage 211, 116443. https://doi.org/10.1016/j.neuroimage.2019.116443.

Carelli, V., Ross-Cisneros, F.N., Sadun, A.A., 2002. Optic nerve degeneration and mitochondrial dysfunction: genetic and acquired optic neuropathies. Neurochem. Int. 40, 573–584. https://doi.org/10.1016/s0197-0186(01)00129-2.

Bullmore, E.d., Sporns, O., 2009. Complex brain networks: graph theoretical analysis of structural and functional systems. Nat. Rev. Neurosci. 10, 186–198. https://doi.org/10.1038/nrn2575.

Cai, S., Huang, K., Kang, Y., Jiang, Y., von Deneen, K.M., Huang, L., 2019. Potential biomarkers for distinguishing people with Alzheimer's disease from cognitively intact elderly based on the rich-club hierarchical structure of white matter networks. Neurosci. Res. 144, 56–66. https://doi.org/10.1016/j.neures.2018.07.005.

Ceranic, B., Luxon, L.M., 2004. Progressive auditory neuropathy in patients with Leber's hereditary optic neuropathy. J. Neurol. Neurosurg. Psychiatry 75, 626–630. https://doi.org/10.1136/jnnp.2003.017673.

Chang, M., 2018. Leber's hereditary optic neuropathy misdiagnosed as optic neuritis and Lyme disease in a patient with multiple sclerosis. BMJ Case Rep 11, e227109. https://doi.org/10.1136/bcr-2018-227109.

Collin, G., Scholtens, L.H., Kahn, R.S., Hillegers, M.H.J., van den Heuvel, M.P., 2017. Affected anatomical rich club and structural-functional coupling in young offspring of schizophrenia and bipolar disorder patients. Biol. Psychiatry 82, 746–755. https://doi.org/10.1016/j.biopsych.2017.06.013.

Crossley, N.A., Mechelli, A., Scott, J., Carletti, F., Fox, P.T., McGuire, P., Bullmore, E.T., 2014. The hubs of the human connectome are generally implicated in the anatomy of brain disorders. Brain 137, 2382–2395. https://doi.org/10.1093/brain/awu132.

Cui, S., Yang, L., Jiang, H., Peng, J., Shang, J., Wang, J., Zhang, X., 2020. Clinical Features of Chinese Sporadic Leber Hereditary Optic Neuropathy Caused by Rare Primary mtDNA Mutations. J. Neuroophthalmol. 40, 30–36. https://doi.org/10.1097/WNO.0000000000000799.

Fan, L., Li, H., Zhuo, J., Zhang, Y.u., Wang, J., Chen, L., Yang, Z., Chu, C., Xie, S., Laird, A.R., Fox, P.T., Eickhoff, S.B., Yu, C., Jiang, T., 2016. The Human Brainnetome Atlas: A New Brain Atlas Based on Connectional Architecture. Cereb. Cortex 26, 3508–3526. https://doi.org/10.1093/cercor/bhw157.

Farrell, J.A.D., Landman, B.A., Jones, C.K., Smith, S.A., Prince, J.L., van Zijl, P.C.M., Mori, S., 2007. Effects of signal-to-noise ratio on the accuracy and reproducibility of diffusion tensor imaging-derived fractional anisotropy, mean diffusivity, and principal eigenvector measurements at 1.5 T. J. Magn. Reson. Imaging 26, 756–767. https://doi.org/10.1002/jmri.21053.

Gaier, E.D., Gittinger, J.W., Cestari, D.M., Miller, J.B., 2016. Peripapillary capillary dilation in leber hereditary optic neuropathy revealed by optical coherence tomographic angiography. JAMA Ophthalmol 134, 1332. https://doi.org/10.1001/jamaophthalmol.2016.3593.

Gropman, A., Chen, T.-J., Perng, C.-L., Krasnewich, D., Chernoff, E., Tifft, C., Wong, L.-J., 2004. Variable clinical manifestation of homoplasmic G14459A mitochondrial DNA mutation. Am. J. Med. Genet. A 124A, 377–382. https://doi.org/10.1002/ajmg.a.20456.

Hasson, U., Andric, M., Atilgan, H., Collignon, O., 2016. Congenital blindness is associated with large-scale reorganization of anatomical networks. Neuroimage 128, 362–372. https://doi.org/10.1016/j.neuroimage.2015.12.048.

Jeurissen, B., Descoteaux, M., Mori, S., Leemans, A., 2019. Diffusion MRI fiber tractography of the brain. NMR Biomed. 32, e3785. https://doi.org/10.1002/nbm.v32.410.1002/nbm.3785.

Kim, D.J., Min, B.K., 2020. Rich-club in the brain's macrostructure: Insights from graph theoretical analysis. Comput. Struct. Biotechnol. J. 18, 1761–1773. https://doi.org/10.1016/j.csbj.2020.06.039.

Leng, Y., Liu, Y., Fang, X., Li, Y., Yu, L., Yuan, Y., Wang, Z., 2015. The mitochondrial DNA 10197 G > A mutation causes MELAS/Leigh overlap syndrome presenting with acute auditory agnosia. Mitochondrial DNA 26, 208–212. https://doi.org/10.3109/19401736.2014.905860.

Li, J., Liu, Y., Qin, W., Jiang, J., Qiu, Z., Xu, J., Yu, C., Jiang, T., 2013. Age of onset of blindness affects brain anatomical networks constructed using diffusion tensor tractography. Cereb. Cortex 23, 542–551. https://doi.org/10.1093/cercor/bhs034.

Liu, Y., Yu, C., Liang, M., Li, J., Tian, L., Zhou, Y., Qin, W., Li, K., Jiang, T., 2007. Whole brain functional connectivity in the early blind. Brain 130, 2085–2096. https://doi.org/10.1093/brain/awm121.

Long, M., Wang, L., Tian, Q., Ding, H., Qin, W., Shi, D., Yu, C., 2019. Brain white matter changes in asymptomatic carriers of Leber's hereditary optic neuropathy. J. Neurol. 266, 1474–1480. https://doi.org/10.1007/s00415-019-09284-2.

Maier-Hein, K.H., Neher, P.F., Houde, J.C., Cote, M.A., Garyfallidis, E., Zhong, J., Chamberland, M., Yeh, F.C., Lin, Y.C., Ji, Q., Reddick, W.E., Glass, J.O., Chen, D.Q., Feng, Y., Gao, C., Wu, Y., Ma, J., Renjie, H., Li, Q., Westin, C.F., Deslauriers-Gauthier, S., Gonzalez, J.O.O., Paquette, M., St-Jean, S., Girard, G., Rheault, F., Sidhu, J., Tax, C.M.W., Guo, F., Mesri, H.Y., David, S., Froeling, M., Heemskerk, A. M., Leemans, A., Bore, A., Pinsard, B., Bedetti, C., Desrosiers, M., Brambati, S., Doyon, J., Sarica, A., Vasta, R., Cerasa, A., Quattrone, A., Yeatman, J., Khan, A.R., Hodges, W., Alexander, S., Romascano, D., Barakovic, M., Auria, A., Esteban, O., Lemkaddem, A., Thiran, J.P., Cetingul, H.E., Odry, B.L., Mailhe, B., Nadar, M.S., Pizzagalli, F., Prasad, G., Villalon-Reina, J.E., Galvis, J., Thompson, P.M., Requejo, F. S., Laguna, P.L., Lacerda, L.M., Barrett, R., Dell'Acqua, F., Catani, M., Petit, L., Caruyer, E., Daducci, A., Dyrby, T.B., Holland-Letz, T., Hilgetag, C.C., Stieltjes, B., Descoteaux, M., 2017. The challenge of mapping the human connectome based on diffusion tractography. Nat Commun 8, 1349. https://doi.org/10.1038/s41467-017-01285-x.

Manners, D.N., Rizzo, G., La Morgia, C., Tonon, C., Testa, C., Barboni, P., Malucelli, E., Valentino, M.L., Caporali, L., Strobbe, D., Carelli, V., Lodi, R., 2015. Diffusion tensor imaging mapping of brain white matter pathology in mitochondrial optic neuropathies. AJNR Am. J. Neuroradiol. 36, 1259–1265. https://doi.org/10.3174/ajnr.A4272.

Maslov, S., Sneppen, K., 2002. Specificity and stability in topology of protein networks. Science 296, 910–913. https://doi.org/10.1126/science.1065103.

Mejia-Vergara, A.J., Seleme, N., Sadun, A.A., Karanjia, R., 2020. Pathophysiology of conversion to symptomatic leber hereditary optic neuropathy and therapeutic implications: a review. Curr. Neurol. Neurosci. Rep. 20 https://doi.org/10.1007/s11910-020-01032-8.

Mercuri, M.A., White, H., Oliveira, C., 2017. Vision Loss and Symmetric Basal Ganglia Lesions in Leber Hereditary Optic Neuropathy. J Neuroophthalmol 37, 411–413. https://doi.org/10.1097/WNO.0000000000000524.

Milesi, J., Rocca, M.A., Bianchi-Marzoli, S., Petrolini, M., Pagani, E., Falini, A., Comi, G., Filippi, M., 2012. Patterns of white matter diffusivity abnormalities in Leber's hereditary optic neuropathy: a tract-based spatial statistics study. J. Neurol. 259, 1801–1807. https://doi.org/10.1007/s00415-011-6406-1.

Moster, S.J., Moster, M.L., Scannell Bryan, M., Sergott, R.C., 2016. Retinal ganglion cell and inner plexiform layer loss correlate with visual acuity loss in LHON: a longitudinal, segmentation OCT analysis. Invest. Ophthalmol. Vis. Sci. 57, 3872. https://doi.org/10.1167/iovs.15-17328.

Nakaso, K., Adachi, Y., Fusayasu, E., Doi, K., Imamura, K., Yasui, K., Nakashima, K., 2012. Leber's hereditary optic neuropathy with olivocerebellar degeneration due to G11778A and T3394C mutations in the mitochondrial DNA. J. Clin. Neurol. 8, 230. https://doi.org/10.3988/jcn.2012.8.3.230.

Ogawa, S., Takemura, H., Horiguchi, H., Terao, M., Haji, T., Pestilli, F., Yeatman, J.D., Tsuneoka, H., Wandell, B.A., Masuda, Y., 2014. White matter consequences of retinal receptor and ganglion cell damage. Invest. Ophthalmol. Vis. Sci. 55, 6976–6986. https://doi.org/10.1167/iovs.14-14737.

Ostojic, J., Jancic, J., Kozic, D., Semnic, R., Koprivsek, K., Prvulovic, M., Kostic, V., 2009. Brain white matter 1 H MRS in Leber optic neuropathy mutation carriers. Acta Neurol. Belg. 109, 305–309.

Poincenot, L., Pearson, A.L., Karanjia, R., 2020. Demographics of a large international population of patients affected by leber's hereditary optic neuropathy. Ophthalmology 127, 679–688. https://doi.org/10.1016/j.ophtha.2019.11.014.

Qin, W., Zhang, M., Piao, Y., Guo, D., Zhu, Z., Tian, X., Li, K., Yu, C., Yang, Y., 2012. Wallerian degeneration in central nervous system: dynamic associations between diffusion indices and their underlying pathology. PLoS ONE 7, e41441. https://doi.org/10.1371/journal.pone.0041441.

Qin, W., Xuan, Y., Liu, Y., Jiang, T., Yu, C., 2015. Functional connectivity density in congenitally and late blind subjects. Cereb. Cortex 25, 2507–2516. https://doi.org/10.1093/cercor/bhu051.

Rance, G., Kearns, L.S., Tan, J., Gravina, A., Rosenfeld, L., Henley, L., Carew, P., Graydon, K., O'Hare, F., Mackey, D.A., 2012. Auditory function in individuals within Leber's hereditary optic neuropathy pedigrees. J. Neurol. 259, 542–550. https://doi.org/10.1007/s00415-011-6230-7.

Rizzo, G., Tozer, K.R., Tonon, C., Manners, D., Testa, C., Malucelli, E., Valentino, M.L., La Morgia, C., Barboni, P., Randhawa, R.S., Ross-Cisneros, F.N., Sadun, A.A., Carelli, V., Lodi, R., Paul, F., 2012. Secondary post-geniculate involvement in Leber's hereditary optic neuropathy. PLoS ONE 7, e50230. https://doi.org/10.1371/journal.pone.0050230.

Rocca, M.A., Valsasina, P., Pagani, E., Bianchi-Marzoli, S., Milesi, J., Falini, A., Comi, G., Filippi, M., Wang, Y.i., 2011. Extra-visual functional and structural connection abnormalities in Leber's hereditary optic neuropathy. PLoS ONE 6, e17081. https://doi.org/10.1371/journal.pone.0017081.

Saracchi, E., DiFrancesco, J.C., Brighina, L., Marzorati, L., Curtò, N.A., Lamperti, C., Carrara, F., Zeviani, M., Ferrarese, C., 2013. A case of Leber hereditary optic neuropathy plus dystonia caused by G14459A mitochondrial mutation. Neurol Sci 34 (3), 407–408. https://doi.org/10.1007/s10072-012-1013-1.

Schaefer, A.M., McFarland, R., Blakely, E.L., He, L., Whittaker, R.G., Taylor, R.W., Chinnery, P.F., Turnbull, D.M., 2008. Prevalence of mitochondrial DNA disease in adults. Ann. Neurol. 63, 35–39. https://doi.org/10.1002/ana.21217.

Schiavi, S., Petracca, M., Battocchio, M., El Mendili, M.M., Paduri, S., Fleysher, L., Inglese, M., Daducci, A., 2020. Sensory-motor network topology in multiple sclerosis: Structural connectivity analysis accounting for intrinsic density discrepancy. Hum. Brain Mapp. 41, 2951–2963. https://doi.org/10.1002/hbm.24989.

Swenson, R.S., 2006. Review of Clinical and Functional Neuroscience. Dartmouth Medical School.

Takemura, H., Ogawa, S., Mezer, A.A., Horiguchi, H., Miyazaki, A., Matsumoto, K., Shikishima, K., Nakano, T., Masuda, Y., 2019. Diffusivity and quantitative T1 profile

of human visual white matter tracts after retinal ganglion cell damage. Neuroimage Clin. 23, 101826. https://doi.org/10.1016/j.nicl.2019.101826.

Vacchiano, V., Tonon, C., Mitolo, M., Evangelisti, S., Carbonelli, M., Liguori, R., Lodi, R., Carelli, V., La Morgia, C., 2019. Functional MRI study in a case of Charles Bonnet syndrome related to LHON. BMC Neurol 19. https://doi.org/10.1186/s12883-019-1579-9.

van den Heuvel, M.P., Sporns, O., 2011. Rich-club organization of the human connectome. J. Neurosci. 31, 15775–15786. https://doi.org/10.1523/JNEUROSCI.3539-11.2011.

van den Heuvel, M.P., Sporns, O., Collin, G., Scheewe, T., Mandl, R.C.W., Cahn, W., Goñi, J., Hulshoff Pol, H.E., Kahn, R.S., 2013. Abnormal rich club organization and functional brain dynamics in schizophrenia. JAMA Psychiatry 70, 783. https://doi.org/10.1001/jamapsychiatry.2013.1328.

Wang, B., Zhan, Q., Yan, T., Imtiaz, S., Xiang, J., Niu, Y., Liu, M., Wang, G., Cao, R., Li, D., 2019. Hemisphere and Gender Differences in the Rich-Club Organization of Structural Networks. Cereb Cortex 29, 4889-4901.https://doi.org/10.1093/cercor/bhz027.

Wang, L., Fan, K.e., Zhang, Y., Chen, Y., Tian, Q., Shi, D., 2017. Quantitative assessment of optic nerve in patients with Leber's hereditary optic neuropathy using reduced field-of-view diffusion tensor imaging. Eur. J. Radiol. 93, 24–29. https://doi.org/10.1016/j.ejrad.2017.05.025.

Wang, D., Qin, W., Liu, Y., Zhang, Y., Jiang, T., Yu, C., 2014. Altered resting-state network connectivity in congenital blind. Hum. Brain Mapp. 35, 2573–2581. https://doi.org/10.1002/hbm.22350.

Yeh, C.H., Jones, D.K., Liang, X., Descoteaux, M., Connelly, A., 2020. Mapping Structural Connectivity Using Diffusion MRI: Challenges and Opportunities. J. Magn. Reson. Iamaging. https://doi.org/10.1002/jmri.27188.

Yu-Wai-Man, P., Elliott, C., Griffiths, P.G., Johnson, I.J., Chinnery, P.F., 2008. Investigation of auditory dysfunction in Leber hereditary optic neuropathy. Acta. Ophthalmol. 86, 630–633. https://doi.org/10.1111/j.1600-0420.2007.01078.x.

Yu-Wai-Man, P., Turnbull, D.M., Chinnery, P.F., 2002. Leber hereditary optic neuropathy. J. Med. Genet. 39, 162–169. https://doi.org/10.1136/jmg.39.3.162.

Yu-Wai-Man, P., Votruba, M., Burté, F., La Morgia, C., Barboni, P., Carelli, V., 2016. A neurodegenerative perspective on mitochondrial optic neuropathies. Acta Neuropathol. 132, 789–806. https://doi.org/10.1007/s00401-016-1625-2.

Zalesky, A., Fornito, A., Bullmore, E.T., 2010. Network-based statistic: identifying differences in brain networks. Neuroimage 53, 1197–1207. https://doi.org/10.1016/j.neuroimage.2010.06.041.

Zhan, L., Leow, A.D., Jahanshad, N., Chiang, M.-C., Barysheva, M., Lee, A.D., Toga, A.W., McMahon, K.L., de Zubicaray, G.I., Wright, M.J., Thompson, P.M., 2010. How does angular resolution affect diffusion imaging measures? Neuroimage 49, 1357–1371. https://doi.org/10.1016/j.neuroimage.2009.09.057.